Monitoring diclofenac adsorption by organophilic alkylpyridinium bentonites

D. B. França, Pollyana Trigueiro, E.C. Silva Filho, M. G. Fonseca, M. Jaber

Monitoring diclofenac adsorption by organophilic alkylpyridinium bentonites

D.B. França[a,b], P. Trigueiro[c], E.C. Silva Filho[c], M.G. Fonseca[a,b], M. Jaber[d]

[a]*Universidade Federal da Paraíba, Cidade Universitária, s/n - Castelo Branco III, 58051-085, João Pessoa - PB, Brazil.*

[b]*Núcleo de Pesquisa e Extensão - Laboratório de Combustíveis e Materiais (NPE – LACOM).*

[c]*Laboratório Interdisciplinar de Materiais Avançados (LIMAV), Centro de Tecnologia, UFPI, Teresina, Piaui, Brazil, 64064-260.*

[d]*Sorbonne Université, Laboratoire d'Archéologie Moléculaire et Structurale, CNRS UMR 8220, Tour 23, 3ème étage, couloir 23-33, BP 225, 4 place Jussieu, 75005 Paris, France.*

*Corresponding author: mgardennia@quimica.ufpb.br

Phone/fax +55(83) 3216-7441

Abstract

Organoclays have been applied as efficient adsorbents for pharmaceutical pollutants from aqueous solution. In this work, dodecylpyridinium chloride (C_{12}pyCl) and hexadecylpyridinium chloride (C_{16}pyCl) cationic surfactants were used for the preparation of organobentonites destined for diclofenac sodium (DFNa) adsorption, an anionic drug widely detected in wastewater. The organofunctionalization of the clay samples was performed under microwave irradiation at 50 °C for 5 min with surfactant amounts of 100% and 200% in relation to the cation exchange capacity (CEC) of the pristine bentonite. The amount of incorporated ammonium salts based on CHN elemental analysis was higher for all samples prepared with 200% of the CEC. The basal spacings of the organoclays ranged from 1.54-2.13 nm, indicating the entrance of organic cations into the interlayer spacing of the clay samples, and the spacing depended on the size of the alkyl organic chain. The hydrophobic character of the organobentonites was verified by thermogravimetry and infrared spectroscopy (FTIR). The adsorption isotherms showed that the drug capacity adsorption was influenced by the amount of surfactant incorporated into the bentonite, the packing density and the arrangement of the surfactants in the interlayer spacing. Zeta potential measurements of the organobentonites and FTIR analysis after drug adsorption suggested that electrostatic and nonelectrostatic interactions contributed to the mechanism of adsorption.

Keywords: Organobentonite; microwave heating; adsorption; anti-inflammatory drug; diclofenac

1. Introduction

The presence of pharmaceutical compounds in the environment has become a major concern, particularly due to the consequences related to long exposure, which are still unknown (Lonappan et al., 2016). Diclofenac (2- [2,6-dichlorophenylamino] phenylethanoic acid) is among the main drugs studied in recent years. Diclofenac is a nonsteroidal anti-inflammatory drug often prescribed in human and veterinary medicine and used to reduce inflammation and pains (Acuña et al., 2015; He et al., 2017). As a consequence of its high production and consumption worldwide, both diclofenac and its metabolites have been detected in aquatic bodies in several countries at concentrations of 0.7-4400 ng L^{-1} in surface waters and up to 8.5 μg L^{-1} in wastewater (Lonappan et al., 2016; Scheurell et al., 2009); concentrations of its transformation products are in the range of 0.08 to 1.80 μg L^{-1} (Scheurell et al., 2009). In Brazil, diclofenac was also observed in water in the range of 3.3-785 ng L^{-1} (Starling et al., 2019). Therefore, diclofenac is among the main drugs studied in recent years regarding its identification/detection in aquatic bodies (Biel-Maeso et al., 2018; Starling et al., 2019), removal/degradation (Maia et al., 2019; Mugunthan et al., 2018), and environmental impacts (Klaudia et al., 2019; Moreno-González et al., 2016; Oaks et al., 2004).

Both toxicity and bioaccumulation of diclofenac have been observed for various living aquatic organisms, even at low concentrations (Klaudia et al., 2019; Moreno-González et al., 2016), and diclofenac was identified as the cause of mortality and decline of the vulture population in Pakistan (Oaks et al., 2004). Some studies have observed that diclofenac metabolites can be generated through biotransformation in living organisms or through exposure to sunlight, and some of them are even more toxic than pure diclofenac (Bonnefille et al., 2018; Klaudia et al., 2019).

Due to the environmental problems, several diclofenac removal methods have been evaluated, such as coagulation, flocculation and activated sludge treatment (Carballa et al.,

2005; Vieno and Sillanpää, 2014); adsorption based on natural or synthetic materials (Andrew Lin et al., 2015; Maia et al., 2019); and degradation through advanced oxidative processes, such as ozonation (Beltrán et al., 2009), photo-Fenton (Pérez-Estrada et al., 2005) and photocatalysis (Mugunthan et al., 2018).

In this context, adsorption is highlighted because of the ease of operation and avoidance of subproducts. Organophilic clay minerals have been applied as efficient adsorbents for drug removal from aquatic bodies (Ghemit et al., 2019; Karaman et al., 2012; Maia et al., 2019; Martinez-Costa et al., 2018; Oliveira et al., 2017; Oliveira and Guégan, 2016; Sun et al., 2017a; Thanhmingliana, 2015). The performance of organophilic clays was attributed to a better compatibility with organic pollutants thanks to their hydrophobic nature and to the presence of new sites for adsorption (Oliveira and Guégan, 2016; Zhuang et al., 2019, 2018). Therefore, modified clays with surfactants containing an aromatic ring in their structure have been applied for the adsorption of different pollutants, such as phenolic compounds (Luo et al., 2015), aniline (Gu et al., 2014), bisphenol A (Yang et al., 2016), naphthalene and phenanthrene (Changchaivong and Khaodhiar, 2009). The mechanism of interaction involves both π-π interactions between aromatic rings of the surfactant and the rings of the pollutant and other organic interactions (hydrogen bonding, London forces, etc), making these modified clays better adsorbents (Oliveira et al., 2017; Oliveira and Guégan, 2016). Indeed, hexadecylpyridinium chloride was used, commonly applied as an antibacterial agent widely in antiseptic solutions and some personal care products, as well as a preservative in pharmaceutical preparations and in the meat industry as a spray for the control of microbial growth (Herrera et al., 2004; Özdemir et al., 2013).

Furthermore, the adsorption of organic pollutants is improved when the incorporated amount of surfactant is higher than the cationic exchange capacity (CEC) of the clay mineral (Brito et al., 2018; Luo et al., 2018).

In the present study, organoclays were obtained by the organofunctionalization of bentonite, a mineral constituted predominantly by ≥ 50% smectite, most commonly montmorillonite (Mt). Mt is a 2:1 phyllosilicate with a general structure of $(M^{x+},nH_2O)(Al^{3+}{}_{2-y}Mg^{2+}{}_{y}Si^{4+}{}_{4}O_{10}(OH)_2$, where Si^{4+} ions are coordinated to four oxygens in tetrahedral sites and Mg^{2+}/Al^{3+} ions are octahedrally coordinated to six oxygens. The hydrated interlayer cations M^{x+} (commonly Na^{+} or Ca^{2+}) balance the negative layer charge due to the isomorphic substitution of Mg^{2+} for Al^{3+} in the octahedral sheet. These interlayer cations can be exchanged by organic cations in water solution, resulting in organophilic bentonite derivatives (Lagaly et al., 2013).

Therefore, in this case, organobentonites were synthesized through microwave (MW) heating in a very short time (5 min) by reaction with two alkylpyridinium surfactants that have aromatic rings in their structure. The influences of the chain length and composition of both molecules on the synthesis of organobentonites, and diclofenac adsorption on modified clay samples was evaluated. The synthetized samples were used for the first time for diclophenac adsorption. The tests of drug adsorption were conducted under different experimental conditions, and the influence of adsorbent dosage, pH, time and initial diclofenac concentration were investigated. New insights in the mechanism of drug/solid adsorption were also suggested based on characterization of the adsorbents after drug adsorption.

2. Experimental

2.1 Materials

A sodium bentonite sample (BentNa), CEC 74.64 cmol(+)/kg, was supplied by Bentonise Bentonita Company, Brazil. The chemical composition of the bentonite was as follows: SiO_2 (52.98%), Al_2O_3 (18.35%), Fe_2O_3 (3.96%), TiO_2 (0.18%), CaO (0.01%), MgO

(2.47%), Na_2O (2.56%), K_2O (0.22%) and fire loss 18.59% (Cavalcanti et al., 2019). 1-Dodecylpyridinium chloride hydrate (C_{12}pyCl) and hexadecylpyridinium chloride monohydrate (C_{16}pyCl) with purity grades of 98% and 99%, respectively, were supplied by Sigma-Aldrich and used as received. Diclofenac sodium salt (CAS number 15307-79-6, MM = 318.13 g mol^{-1} and pKa 4.1) was purchased from Sigma-Aldrich.

2.2 Preparation of the alkylpyridinium bentonites

Organobentonites were synthesized based on a previous procedure (Brito et al., 2018). Initially, two solutions of the salts were prepared in concentrations corresponding to 100 and 200% of the CEC of the bentonite. A sample of 4.0 g of BentNa was suspended in 100 mL of each surfactant solution in a Teflon vessel reactor and heated in a microwave reactor (IS-TEC MW reactor model RMW-1, Brazil, with a power of 1100 W and 2.45 GHz) for 5 min at 50 °C. The obtained solids were recovered by centrifugation at 10000 rpm, washed with distilled water until testing negative for chlorite with 0.01 mol L^{-1} $AgNO_3$ and dried in an oven for at least 24 h at 50 °C.

2.3 Diclofenac sorption

The test of diclofenac adsorption followed a previous method (Brito et al., 2018; França et al., 2019), by which the influences of the medium pH (6.0-10.0), dosage of the solid (25-400 mg), time (0.5 – 120 min) and drug initial concentration (1-500 mg L^{-1}) were evaluated.

Batch tests were performed at 30 °C by using samples of organobentonites dispersed in 20 mL of diclofenac solution. This temperature is the medium temperature found for Brazilian aquatic bodies. After each test, the solids were recovered by centrifugation, and the diclofenac concentrations were monitored by UV-Vis molecular spectrometry (Shimadzu

spectrometer model TCC-240 240) at 276 nm (Ghemit et al., 2019). The amount of adsorbed drug (q) was calculated as established in Eq. 1:

$$q = \frac{(C_i - C_e)V}{m} \qquad (1)$$

where C_i and C_e are the drug concentrations before and after adsorption (mg L^{-1}), respectively, V is the total volume of drug solution (L) and m is the mass of the solid (g).

To investigate pH, 50 mg of solids was reacted with 20 mL of 100 mg L^{-1} diclofenac solution for 24 h. The pH was adjusted with 0.05 mol L^{-1} NaOH or HNO_3 solutions.

Tests for the dosage of solids were monitored at optimum pH under the same conditions described.

Tests for different times of interaction were conducted with the fixed mass obtained in the solid dosage tests and at optimum pH for times in the range of 0.5-120 min.

Finally, the initial diclofenac concentrations were evaluated in the range of 1-500 mg L^{-1} at the optimized pH, dosage of solids and time of contact.

All experiments were performed in triplicate.

2.4 Kinetic and equilibrium models

The experimental data were adjusted to fit the following kinetic models: pseudo-first-order (Lagergren, 1898), pseudo-second-order (Ho and McKay, 1999) and simplified Elovich equation (Chien and Clayton, 1984), assuming $\alpha\beta t >> 1$, (see Eqs. 1 to 3 in Supplementary Material SI1).

The equilibrium isotherms were analyzed with the Langmuir (Langmuir, 1918), Freundlich (Freundlich, 1906) and Temkin (Temkin and Pyzhev, 1940) models (see Eqs. 4-6 in Supplementary Material SI1).

The standard deviation (SD-root mean square error), Eq. 2, was used to verify which equation models were best suited to describe the experimental data (Lima et al., 2015).

$$SD = \sqrt{\frac{1}{n_p - p}\sum_i^n (q_{i,exp} - q_{i,model})^2} \qquad (2)$$

where $q_{i,\mathrm{exp}}$ and $q_{i,\mathrm{model}}$ are the experimental adsorbed drug amount and theoretical amount obtained by the kinetic models, n_p is the number of performed experiments, and p is the number of parameters of the fitted model.

2.5 Characterizations

X-ray diffraction (XRD) analyses were conducted on a Shimadzu XD3A model diffractometer with Cu$K\alpha$ radiation and a fixed power source (40 kV and 30 mA). FTIR spectra were recorded in the 4000-400 cm^{-1} region by a Shimadzu IR Prestige-21 model; the samples were dispersed in KBr pellets, and a resolution of 4 cm^{-1} and accumulation of 20 scans were used for each run. Thermogravimetry data for the solids were obtained using an SDT Q600 V20.9 Build 20 thermal analyzer with a heating rate of 10 °C min^{-1} under 100 mL min^{-1} of argon flow in the range of 30 to 900 °C. CHN elemental analysis was obtained by using a Perkin-Elmer PE-2400 microelemental analyzer. Chloride was analyzed by titration: samples of 100 mg in triplicate was suspended in 0.01 mol L^{-1} $NaNO_3$ for 24 h at 25 ^{o}C. The dispersions were centrifuged and the procedure was repeated 3 times to ensure the exchange of Cl^- by NO_3^-. After centrifugation, aliquots of 10 mL of supernatant were titrated with standard $AgNO_3$ solution (Skoog et al., 2012). Zeta potential (ζ) was measured using a Zetasizer Nano Zs (Malvern Instruments) for isoelectric titration through pH titration. The pH of the solutions was adjusted with 0.100 mol L^{-1} NaOH or 0.500 mol L^{-1} HNO_3.

3. Results and discussion

3.1 X-ray diffraction

The XRD pattern of BentNa (Figure SM1a) showed smectite with sodium montmorillonite (Mt) as the predominant phase and impurities of quartz (Q) and muscovite (M), in agreement with ICDD cards 00.029.1498, 00.058.2036 and 01.070.8055 and previous studies (Cavalcanti et al., 2019; Queiroga et al., 2019). Characteristic reflections of Mt at 2θ = 7.37° suggested a basal spacing (d_{001}) of 1.12 nm, as further indicated by additional reflections at 2θ values of 19.6°, 28.3°, 35.0° and 61.8°.

The intercalation of alkylpyridinium cations was confirmed by the increase in basal spacings to 1.56, 1.74, 1.66 and 2.13 nm for Bent-C_{12}py-100%, Bent-C_{16}py-100%, Bent-C_{12}py-200% and Bent-C_{16}-py200% (Figure SM1), respectively. The results indicated that higher values were observed for solids prepared with 200% of the CEC and a longer organic chain of the salt (Changchaivong and Khaodhiar, 2009; Greenland and Quirk, 1962; Muñoz-Shugulí et al., 2019).

Studies have established that the size of the organic chain and the intercalated amount determine the arrangement of surfactants in the interlayer spacing. For example, $C_{16}py^+$ monolayer (d_{001} = 1.32~1.47 nm), bilayer (d_{001} = 1.68~1.78 nm) and pseudotrilayer (d_{001} = 2.14~2.20 nm) arrangements in the gallery spacing of montmorillonite have been proposed (Meleshyn and Bunnenberg, 2006). Based on the size of the surfactant molecules and the final basal spacings (Chen et al., 2005; Luo et al., 2018), monolayer arrangement occurred for Bent-C_{12}py-100%, bilayer arrangement occurred for Bent-C_{12}py-200% and Bent-C_{16}py-100%, and pseudotrilayer arrangement occurred for Bent-C_{16}py-200%, as illustrated in Figure SM2.

The XRD results were compared with previous studies that considered the synthesis of organobentonites by using conventional and microwave heating with the same proportion of surfactant adopted in the present work (Table SM1). The obtained values for Bent-C_{16}py are close to those obtained by (Schampera and Dultz, 2009) and Muñoz-Shugulí et al. (2019) using conventional heating at times of 20 and 1 h at 60 ^{o}C, respectively. However, divergent values were also observed and were associated with the different CECs of the pristine bentonites used (He et al., 2014) different conditions of synthesis. Therefore, the studies showed that aspects such as washing and drying (Luo et al., 2016) and the nature of the interlayer cations (Volzone et al., 2002) can influence the final basal spacing and the amount of intercalated surfactant.

3.2 CHNCl elemental analysis

The amount of incorporated surfactant in the bentonite was determined based on C and N elemental analysis (Table 1); the values were close to the CEC (~ 90% of the initial salt concentration) for Bent-C_{12}py-100% and Bent-C_{16}py-100% and were near that for montmorillonites modified with $C_{16}py^{+}$ using 100% of the CEC by conventional heating (Schampera and Dultz, 2009).

For the organobentonites obtained using 200% of the CEC of BentNa, only Bent-C_{16}py-200% exhibited a value higher than the CEC (112.4%), while C_{12}py-200% exhibited a value of 93.3%. The excess of surfactant in Bent-C_{16}py-200% was incorporated as the ion pair C_{16}pyCl through hydrophobic interactions between the alkyl tails of the organic chain (Luo et al., 2018; Meleshyn and Bunnenberg, 2006), and was further verified by the presence of the chloride in the organoclays (Table 1). No Cl^{-} ions were detected in other organobentonites (Bent-C_{12}py-100%, Bent-C_{16}py-100% and Bent-C_{12}py-200%).

The better affinity of bentonite for surfactants with longer organic chains was related to an increase in the contribution of Van der Waals interactions and a decrease in the hydration enthalpy of the organic salt, favoring intercalation (Teppen and Aggarwal, 2007).

This result suggested that the packing densities of the groups in the solids can be influenced by the amount of intercalated molecules.

3.3 Infrared spectroscopy

Infrared spectra were used to monitor the organofunctionalization of the bentonite; therefore, the spectra of the pristine and modified solids are shown in Figure SM3. For sodium bentonite, typical bands were detected at 3632 cm^{-1} and 3440 cm^{-1}, assigned to the hydroxyl stretching of structural M-OH (M = Al^{3+}, Mg^{2+} or Fe^{3+}) and silanol. The bending of water molecules was also observed at 1638 cm^{-1} (Slaný et al., 2019).

For the region below 1200 cm^{-1}, bands at 1115 and 1042 cm^{-1} were related to Si-O stretching, and bands at 915-847 cm^{-1} were due to AlMOH deformation (M = Al, Fe or Mg) (Slaný et al., 2019). The presence of quartz impurities was confirmed by the Si-O deformation at 798 cm^{-1}. Other bands at 620, 519 and 465 cm^{-1} were assigned to Al-O/Si-O, Al-O-Si and Si-O-Si deformations, respectively, and are characteristic of montmorillonite (Slaný et al., 2019).

The intercalation of the surfactants in the clay minerals was accompanied by the appearance of new bands in the range of 3136-3096 cm^{-1}, attributed to the aromatic CH stretching of pyridine rings, and from 2928-2851 cm^{-1}, related to CH_2 antisymmetric and symmetrical stretching vibrations (Lin-Vien et al., 1991; Luo et al., 2018). The location of the $\nu_{as}(CH_2)$ band at wavelengths higher than those of free surfactants (Table SM2) suggests the

existence of structures with a disordered arrangement of organic cations (gauche conformers) in the interlayer region of the montmorillonite (Chen et al., 2005; Slaný et al., 2019).

The spectra also exhibited a low-intensity band at 1502 cm^{-1} associated with C=C vibrations of aromatic rings, bands at 1486 and 1469 cm^{-1}, associated with CH_3 and CH_2 deformations, respectively and a band at 729 cm^{-1}, related to $(CH_2)_n$ in-phase rocking, characteristic of alkyl chains of surfactants (Lin-Vien et al., 1991; Slaný et al., 2019). The absorptions at 777 and 679 cm^{-1} were assigned to deformation of the pyridine ring (Lin-Vien et al., 1991).

3.4 Thermogravimetry

Thermogravimetry is a useful tool to quantify the amount of organic content in a solid but is also associated with other techniques, such as XRD and FTIR, to characterize how surfactants are confined in the interlayer region (Chen et al., 2005). TG curves (Figure SM4) and the associated mass losses are summarized in Table SM3.

The TG curve of pristine bentonite exhibited two steps of mass loss, the first step at 30-200 °C, attributed to the elimination of the interlayer water and water adsorbed on the surface, and the second from 200-900 °C, associated with the condensation of structural OH (Muñoz-Shugulí et al., 2019).

The organobentonites showed four and five events of mass loss. For all samples, the first event associated with the elimination of water was ≤ 1.2%, suggesting the hydrophobic nature of the organoclays (Muñoz-Shugulí et al., 2019). Additionally, the sum of mass losses of the other events was higher than in the pristine clay and are associated to an exothermal event (Heat flow not presented), which was an indication of the presence of organic moieties in the solids.

The initial temperature associated with the degradation of the organic part decreased as the incorporated amount of surfactant increased and was observed at 182, 175, 174 and 118 °C for the Bent-C12py-100%, Bent-C16py-100% Bent-C12py-200% and Bent-C16py-200% solids, respectively; this degradation finished at 513-520 °C; therefore, the number of decomposition events exhibited within this range depended on the types of interactions (Chen et al., 2005; Muñoz-Shugulí et al., 2019).

Meleshyn and Bunnenberg, (2006) suggested that a lower temperature for the exit of surfactants occurs due to the different arrangements of organic chains in the interlayer spacing of clay samples and is an indication of weaker interactions (lower energy) between the organic cations and the mineral surface. In other words, as the organic cation content increases, the configurations change from monolayer and bilayer to pseudotrilayer, in accordance with the observed results.

Above 520 °C, mass loss was attributed to dehydroxylation (Luo et al., 2018; Muñoz-Shugulí et al., 2019).

3.5 Zeta potential

Zeta potential measurements (Figure SM5) suggested that the point of zero charge (pH_{PZC}) occurred at pH 3.4, 2.5, 4.1 and 8.1 for Bent-C_{12}-100%, Bent-C_{16}-100%, Bent-C_{12}-200% and Bent-C_{16}-200%, respectively. BentNa is negatively charged in all pH ranges. The modification of clay minerals with cationic surfactants promotes a total or partial variation in surface charge, depending on the amount of organic cations incorporated (Brito et al., 2018; Schampera and Dultz, 2009). Therefore, the values of pH_{PZC} observed for Bent-C_{12}-100%, Bent-C_{16}-100% and Bent-C_{12}-200% are probably related to the low amount of surfactant incorporated (~ 90% of the CEC), while the higher value of pH_{PZC} for Bent-C_{16}-200% is

consistent with the excess surfactant adsorbed probably on the basal surface of the bentonite sample, as indicated by the CHNCl and thermogravimetry results.

3.7 Adsorption of diclofenac on the solids

3.7.1 Influence of pH

The effect of pH on the adsorption process has often been evaluated according to the different behaviors presented by drugs and solids in aqueous media (Ghemit et al., 2019; Oliveira et al., 2017). This parameter was analyzed considering the speciation of the diclofenac molecule at different pH values (Figure SM6i) and zeta potential measurements (ζ) (Figure SM5). The results showed that the adsorption depended slightly on the pH (Figure SM6ii); the maximum values were 12.87, 18.19, 25.30 and 39.40 mg g^{-1} for Bent-C_{12}-100%, Bent-C_{16}-100%, Bent-C_{12}-200% and Bent-C_{16}-200%, respectively, at pH 6.0 and were better than those at pH 8 and 10.

Based on the pKa (4.1) of diclofenac, at pH ≥ 6, the anionic form dominates, and the decreased adsorption with increased pH (6-10) for Bent-C_{12}-100%, Bent-C_{16}-100% and Bent-C_{12}-200% can be associated with the repulsion between deprotonated diclofenac and organobentonites (Luo et al., 2015), considering the pH_{PZC} value; at pH < pH_{PZC}, the surface is positively charged, and the surface is negatively charged for pH values above the pH_{PZC}. These results suggested that non-electrostatic interactions contributed to the mechanism of adsorption.

3.7.2 Dosage of the adsorbent

The dosage of the adsorbent (Figure SM7) is important for establishing the best adsorption efficiency of the drug from solution. The adsorption percentages increase

gradually with increased organobentonite mass due to the increase of interaction sites amount (Brito et al., 2018; Ghemit et al., 2019).

The best performance was observed for 300, 200, 150 and 50 mg of Bent-C_{12}-100%, Bent-C_{16}-100%, Bent-C_{12}-200% and Bent-C_{16}-200%, respectively and these dosages were associated with adsorption efficiencies of 88.3, 97.1, 93.5 and 99.5%. The adsorbed amounts per gram of adsorbent (q) were 5.9 mg g^{-1} for Bent-C_{12}py-100%, 9.3 mg g^{-1} for Bent-C_{16}py-100%, 13.0 mg g^{-1} for Bent-C_{12}py-200% and 38.7 mg g^{-1} para Bent-C_{16}py-200% (Figure SM7ii).

3.7.3 Kinetic studies

Adsorption kinetic studies of diclofenac (Figure SM8) were carried out using the masses corresponding to the maximum percentages of diclofenac adsorption obtained in the evaluation of the adsorbent dosage effect at pH 6.0. The isotherms showed rapid adsorption of the drug by the organophilic clays at 60 and 10 min for the solids obtained with 100% and 200% of the CEC, respectively. These results were close to those observed for other organophilic clays used for diclofenac adsorption (Ghemit et al., 2019; Sun et al., 2017a).

The adsorption kinetics were analyzed by nonlinear regression of the isotherms to the pseudo-first-order, pseudo-second-order and Elovich models, whose parameters are summarized in Table 2. In addition to R^2, the fit of the isotherms to the models was also evaluated using the standard deviation (SD) (Lima et al., 2015), which showed a better fit to the Elovich equation for Bent-C_{12}py-100% and Bent-C_{16}py-100% and a better fit to the pseudo-second-order model for Bent-C_{12}py-200% and Bent-C_{16}py-200%. The Elovich model describes the process as chemisorption and considers the heterogeneity of the surface of the adsorbent (Lima et al., 2015).

3.7.4 Adsorption isotherms

The equilibrium isotherms were evaluated at 1-500 mg L^{-1} diclofenac (Figure 1), pH 6 and 60 min. The isotherms for the organobentonites initially showed an increase in adsorbed amount (qe) with increased drug concentration, reaching almost constant values at initial concentrations (Ci) of 350 mg L^{-1} for Bent-C_{16}py-100% and Bent-C_{12}py-200%, 300 mg L^{-1} for Bent-C_{16}py-200% and 450 mg L^{-1} for Bent-C_{12}py-100%.

The maximum adsorption capacities (q_{max}) were 13.02, 19.30, 25.50 and 91.13 mg g^{-1} on Bent-C_{12}py-100%, Bent-C_{16}py-100%, Bent-C_{12}py-200% and Bent-C_{16}py-200%, respectively. The result for pristine bentonite was less than 5% of the reported values (< 5 mg g^{-1}) under the same conditions. These results were also compared with the diclofenac adsorption capacity on other organoclays samples obtained from conventional procedure at time of 15-72 h (Table SM4), and illustrated the good performance of the organobentonites obtained in this study in only 5 min by microwave irradiation. Long time reactions is a limitation for use of organoclays industrial scale (Yapar, 2009), however, the use of microwave irradiation behaved as good alternative for rapid and reproductive preparation of modified clay minerals.

Beyond the low-cost and good efficiency of the organobentonites, the choice of adsorbent depends of other factors such biocompatibility with the ecosystem and their regeneration and recycle (Biswas et al., 2019; Momina et al., 2018), that were not studied in this present case.

Some organoclays exhibited high toxicity (Sarkar et al., 2013; Witthuhn et al., 2005) while others did not showed any toxicity for the original community of soil microorganisms responsible for biodegradation (Abbate et al., 2013), therefore, the toxicity of alkylpyridium bentonites remains still unknown. The antibacterial activities of hexadecylpyridinium-montmorillonites was verified only against some bacteria responsible for infections in humans and animals and food

388 contamination (Herrera et al., 2000; Malachová et al., 2009; Özdemir et al., 2013), and when
389 added to the diet of weaned pigs was proposed as an alternative to antibiotic chlortetracycline
390 for improving growth performance, mucosal architecture and modifying intestinal microflora
391 (Ke et al., 2014). Moreover, some studied observed that these solids can be used as precursor
392 to obtain new materials such as porous clay heterostructures (Zhu et al., 2005) or carbon-clay
393 composites (Jović-Jovičić et al., 2019).

394 Comparing the results for solids modified with the same surfactant, better adsorption
395 was observed for adsorbents with a higher organic content and basal spacing, for example
396 organobentonite prepared with 100 and 200% of the CEC. Similar results were observed in
397 previous studies for organobentonites prepared with hexadecyltrimethylammonium (Ghemit
398 et al., 2019; Sun et al., 2017a).

399 In addition, the nature of the surfactant, packing density, amount incorporated and
400 organization of the organic cations in the interlayer region can influence drug adsorption in
401 aqueous media (Oliveira et al., 2017; Oliveira and Guégan, 2016). Organic pollutant
402 adsorption on organophilic pyridinium montmorillonites is dependent on these cited effects
403 (Chen et al., 2005; Gu et al., 2014; Luo et al., 2015), as has also been observed for inorganic
404 pollutants (Luo et al., 2017). The cited studies demonstrate that the different characteristics of
405 organoclays influence their affinity for pollutants and, in some cases, their interaction
406 mechanisms.

407 In this present case, the obtained q_e values for diclofenac adsorption on Bent-C_{12}py-
408 100%, Bent-C_{16}py-100% and Bent-C_{12}py-100% were also influenced by the packing density
409 and the organization of alkylpyridinium cations inside the interlayer spacing since these
410 adsorbents presented lower amounts of incorporated surfactants (close to the CEC) but
411 different d_{001} and cation sizes.

412 The data were evaluated according to the Langmuir, Freundlich and Temkin
413 adsorption models, and the parameters obtained are summarized in Table 3. From the values
414 of R^2 and SD, the experimental data were better fit by the Langmuir model for all
415 organobentonitas, indicating that chemisorption can be the preponderant mechanism involved
416 in the diclofenac adsorption. Langmuir model is based on the existence of homogenous
417 adsorption sites. The adjustment was better for Bent-C_{12}py-100% sample (higher R^2 and
418 lower SD), which is an indication of more uniformed distribution of the adsorptions sites of
419 the same nature.
420

421 **3.7.5 Characterization of the drug/clay mineral hybrids**

422 **3.7.5.1 X-ray diffraction**

423 XRD patterns of the drug/clay mineral hybrids (Figure 2) obtained with 10, 100 and
424 500 mg L^{-1} of initial drug concentrations did not present alterations in the basal spacing, as
425 observed in the literature for organophilic montmorillonites (Oliveira et al., 2017; Oliveira
426 and Guégan, 2016; Sun et al., 2017a).

427 The adsorption of a drug in the interlayer region of a clay mineral can drive the
428 rearrangement of the surfactant molecules without changes in the value of the basal spacing
429 (Meleshyn and Bunnenberg, 2006; Oliveira et al., 2017; Oliveira and Guégan, 2016; Sun et
430 al., 2017a). For the sample Bent-C_{12}py-200% (d_{001} = 1.66 nm), the packaging density was
431 higher than that for Bent-C_{12}py-100% (d_{001} = 1.56 nm). Consequently, the entrance of the
432 drug would be more difficult for Bent-C_{12}py-200%, however the adsorption was higher for
433 this sample. It more reasonable that the drug did not access more internal adsorption sites.

434 For Bent-C_{16}py-200%, the behavior was different once the basal spacing was 2.13 nm,
435 the amount of organic salt in the solid was higher than the CEC (0.84 mmol g^{-1}) associated

with the presence of the C_{16}pyCl ionic pair. Therefore, the presence of chloride in the equilibrium solution after drug adsorption was a strong indication of another mechanism for adsorption, such as anion exchange between the Cl^- ions and anionic drug. Similar results have also been described previously in perchlorate adsorption (Chitrakar et al., 2012; Luo et al., 2016). The literature shows that Cl^- ions in $C_{16}py^+$-modified montmorillonite were located near the mid plane of the interlayer space (Meleshyn and Bunnenberg, 2006) and are therefore accessible adsorption sites for anionic species, such as diclofenac.

3.7.5.2 Infrared spectroscopy

For better analysis of the results, the infrared spectra of the free drug and drug/solid hybrids prepared at 10, 100 and 500 mg L^{-1} diclofenac were divided into three regions, (Figures 3 and SM9). Therefore, infrared spectra in the region of 4000-2750 cm^{-1} showed diclofenac bands at 3388 and 2357 cm^{-1} assigned to free and bound N-H stretching, respectively, the latter through intramolecular hydrogen bonds (N-H···O) (Kovala-Demertzi et al., 1993; Lin-Vien et al., 1991). The bands at 3080 and 3036 cm^{-1} were attributed to ν(C-H)$_{aromatic}$, and those at 2971 and 2897 cm^{-1} were due antisymmetric and symmetric aliphatic CH_2 stretching (Lin-Vien et al., 1991). For the drug/Bent-C_{16}-200% hybrid, the initial band of OH stretching of water at 3410 cm^{-1} was shifted to 3430-3422 cm^{-1} for solids with 3.71 mg g^{-1} (C_i = 10 mg L^{-1}) and 91.13 mg g^{-1} (C_i = 500 mg L^{-1}). For the other solids with diclofenac, no alteration was observed in this region.

For region 2 (1750-1250 cm^{-1}), diclofenac presents typical bands associated with aromatic ring stretching at 1603 and 1556 cm^{-1}, a band at 1507 and 1500 cm^{-1} assigned to C-N-H bending of the secondary amine and C-H rock of aromatic rings, band at 1468 cm^{-1} due to C-N stretching and C-H rock (aromatic ring), and bands at 1452 and 1305 cm^{-1} attributed to

461 CH_2 bending (Iliescu et al., 2004; Lin-Vien et al., 1991). The samples with adsorbed
462 diclofenac showed broader bands of aromatic ring stretching at 1558 cm^{-1} and CH_2 bending at
463 1455 cm^{-1}.

464 The diclofenac infrared spectrum also presents bands at 1575 and 1400 cm^{-1}, assigned
465 to antisymmetric and symmetrical stretching of carboxylate group, respectively. The observed
466 wavenumber variation $\Delta\nu(COO^-)$ of 175 cm^{-1} is characteristic of the drug in ionic form
467 (Kovala-Demertzi et al., 1993). Therefore, both bands were detected at 1580~1584 cm^{-1} and
468 1378~1370 cm^{-1} for all organobentonite/drug solid samples, suggesting that $-COO^-$ groups
469 were also involved, possibly through electrostatic interaction (Sun et al., 2017b, 2017c).

470 The occurrence of electrostatic interactions between diclofenac and Bent-C_{12}-100%,
471 Bent-C_{16}-100% and Bent-C_{12}-200% is not probable due to the negative charges of the
472 surfaces at pH 6.0. Similar behavior was observed for an organophilic montmorillonite
473 obtained using a concentration of C_{16}pyCl at 92% of the CEC (Luo et al., 2017). Although the
474 surface was negatively charged and the amount was lower than the CEC, ReO_4^- was adsorbed.
475 The proposed interaction was associated with the desorption of the surfactant weakly bound
476 to montmorillonite, capturing of anions in solution and subsequent adsorption of $C_{16}py^+ReO_4^-$
477 on the external surface by hydrophobic interactions. This same mechanism was also
478 suggested for the adsorption of ClO_4^- anions on $C_{16}py^+$-montmorillonite (Luo et al., 2016).

479 Finally, region 3 of the FTIR spectrum for free diclofenac presented bands at 766, 746
480 and 714 cm^{-1} assigned to C-H deformation (Kovala-Demertzi et al., 1993) and characteristic
481 of 1,2-disubstituted and 1,2,3-trisubstituted aromatic rings (Iliescu et al., 2004), and the band
482 at 635 cm^{-1} is characteristic of ring deformation modes (Lin-Vien et al., 1991). For this
483 region, only Bent-C_{16}-200% exhibited a shoulder at 746 cm^{-1} when a high initial drug
484 concentration was used.

485

3.7.6 Mechanism of drug interaction

The new properties of the organophilic clays were attributed to a change in character from hydrophilic to hydrophobic, anion exchange as a consequence of the incorporation of excess surfactant and different packing densities and arrangements of the organic cations in the interlayer region, which favor interactions with pollutants (Oliveira et al., 2017; Oliveira and Guégan, 2016). Thus, the different characteristics presented by each solid contributed in several forms to diclofenac adsorption due to the different affinities, as observed in the values of q_{max}.

A theoretical study realized by Meleshyn and Bunnenberg (2006) indicated that interlayer anion sorption on montmorillonite modified with C_{16}pyCl occurs only for higher surfactant contents and basal spacings (2.1~2.2 nm) and consequently when a pseudotrimolecular form is obtained. In this condition, chloride can be accommodated between the layers as a counter ion of $C_{16}py^+$ or sodium cations. Several works have shown that some of the interlayer cations of pristine bentonite remain in the bentonite structure even when the amount of $C_{16}py^+$ incorporated is equal to or higher than the CEC and act as cation or anion exchange sites (Chitrakar et al., 2012; Luo et al., 2016), in agreement with the theoretical study (Meleshyn and Bunnenberg, 2006).

Based on the CHNCl results, the amount of surfactant higher than the CEC and the presence of chloride ions (0.154 mmol g^{-1}) were observed only for Bent-C_{16}py-200%. In this case, 0.145 mmol g^{-1} Cl^- was detected in the equilibrium solution after diclofenac adsorption, which was half of the maximum diclofenac adsorbed (0.291 mmol g^{-1}).

For the other solids, although the amount of alkylpyridinium cation incorporated was lower than the CEC of the pristine bentonite, the FTIR results also suggested electrostatic between the incorporated surfactant (pyridinium) and the carboxylate groups of diclofenac.

However, the influence of the pH on drug adsorption is not electrostatic in nature and contributes to organophilic (alkyl groups of the salt and ring of the drug) and π-π interactions, the latter between the pyridine rings and the aromatic rings of the pollutant. In particular, interactions involving π electrons have often been described in the adsorption of aromatic compounds by pyridinium organophilic clays (Changchaivong and Khaodhiar, 2009; Gu et al., 2014; Luo et al., 2015; Yang et al., 2016), and for diclofenac adsorption by benzyldimethyltetradecylammonium-montmorillonite (Oliveira et al., 2017; Oliveira and Guégan, 2016). A general scheme of the proposed interaction mechanisms of drug adsorption on organobentonites was based on obtained results and also in the literature. Depending of the sample, at least four different contributions were involved in the diclofenac adsorption as illustrated in Figure 4.

4. Conclusion

The organic modification of bentonite with alkylpyridinium cations through microwave heating resulted in organophilic clays with different characteristics, which were dependent on the amount of surfactant and the size of the organic chain, as shown in the CHN and XRD results. The use of microwave for organophilization of bentonites with both surfactants at time of 5 min at 50 ^{o}C was a promising technique.

As a consequence, the organobentonites exhibited different diclofenac adsorption capacity from aqueous solution, which were probably influenced by the amount of incorporated surfactant, the packing density and different arrangements of the organic moieties in the interlayer region. The differences between these factors determine the degree of affinity of the hybrids for the anionic drug on the surface due to the different adsorption sites.

The drug/organoclay interaction consisted of electrostatic, organophilic and, possibly, π-π interactions for all functionalized bentonites. The best performance for diclofenac adsorption was 91.13 mg g^{-1} for Bent-C_{16}py-200% due to the excess of surfactant incorporated. This present study demonstrated the versatility of these solids for anionic species or even neutral species, considering the presence of different interaction sites.

Acknowledgement

CNPq is acknowledged for financial support in the form of research fellowships awarded to M.G. Fonseca (grants 310921-2017-1 and 431727/2016-3) and D.B França (140661/2017-4). Prof Dalva L.A. Farias (IQ/USP) for her kindly help in Raman spectroscopy.

References

Abbate, C., Ambrosoli, R., Minati, J.L., Gennari, M., Arena, M., 2013. Metabolic and molecular methods to evaluate the organoclay effects on a bacterial community. Environ. Pollut. 179, 39–44. https://doi.org/10.1016/j.envpol.2013.04.012

Acuña, V., Ginebreda, A., Mor, J.R., Petrovic, M., Sabater, S., Sumpter, J., Barceló, D., 2015. Balancing the health benefits and environmental risks of pharmaceuticals: Diclofenac as an example. Environ. Int. 85, 327–333. https://doi.org/10.1016/j.envint.2015.09.023

Andrew Lin, K.-Y., Yang, H., Lee, W.-D., 2015. Enhanced removal of diclofenac from water using a zeolitic imidazole framework functionalized with cetyltrimethylammonium bromide (CTAB). RSC Adv. 5, 81330–81340. https://doi.org/10.1039/C5RA08189K

Beltrán, F.J., Pocostales, P., Alvarez, P., Oropesa, A., 2009. Diclofenac removal from water with ozone and activated carbon. J. Hazard. Mater. 163, 768–776. https://doi.org/10.1016/J.JHAZMAT.2008.07.033

Biel-Maeso, M., Baena-Nogueras, R.M., Corada-Fernández, C., Lara-Martín, P.A., 2018. Occurrence, distribution and environmental risk of pharmaceutically active compounds (PhACs) in coastal and ocean waters from the Gulf of Cadiz (SW Spain). Sci. Total Environ. 612, 649–659. https://doi.org/10.1016/J.SCITOTENV.2017.08.279

Biswas, B., Warr, L.N., Hilder, E.F., Goswami, N., Rahman, M.M., Churchman, J.G., Vasilev, K., Pan, G., Naidu, R., 2019. Biocompatible functionalisation of nanoclays for improved environmental remediation. Chem. Soc. Rev. 48, 3740–3770. https://doi.org/10.1039/C8CS01019F

565 Bonnefille, B., Gomez, E., Courant, F., Escande, A., Fenet, H., 2018. Diclofenac in the
566 marine environment: A review of its occurrence and effects. Mar. Pollut. Bull. 131, 496–
567 506. https://doi.org/10.1016/j.marpolbul.2018.04.053

568 Brito, D.F., Silva Filho, E.C., Fonseca, M.G., Jaber, M., 2018. Organophilic bentonites
569 obtained by microwave heating as adsorbents for anionic dyes. J. Environ. Chem. Eng. 6,
570 7080–7090. https://doi.org/10.1016/j.jece.2018.11.006

571 Carballa, M., Omil, F., Lema, J.M., 2005. Removal of cosmetic ingredients and
572 pharmaceuticals in sewage primary treatment. Water Res. 39, 4790–4796.
573 https://doi.org/10.1016/J.WATRES.2005.09.018

574 Cavalcanti, G.R.S., Fonseca, M.G., da Silva Filho, E.C., Jaber, M., 2019.
575 Thiabendazole/bentonites hybrids as controlled release systems. Colloids Surfaces B
576 Biointerfaces 176, 249–255. https://doi.org/10.1016/j.colsurfb.2018.12.030

577 Changchaivong, S., Khaodhiar, S., 2009. Adsorption of naphthalene and phenanthrene on
578 dodecylpyridinium-modified bentonite. Appl. Clay Sci. 43, 317–321.
579 https://doi.org/10.1016/j.clay.2008.09.012

580 Chen, B., Zhu, L., Zhu, J., Xing, B., 2005. Configurations of the bentonite-sorbed
581 myristylpyridinium cation and their influences on the uptake of organic compounds.
582 Environ. Sci. Technol. 39, 6093–6100. https://doi.org/10.1021/es0502674

583 Chien, S.H., Clayton, W.R., 1984. Application of Elovich equation to the kinetics of
584 phosphate release and sorption in soils[1]. Soil Sci. Soc. Am. J. 44, 265–268.
585 https://doi.org/10.2136/sssaj1980.03615995004400020013x

586 Chitrakar, R., Makita, Y., Hirotsu, T., Sonoda, A., 2012. Montmorillonite modified with
587 hexadecylpyridinium chloride as highly efficient anion exchanger for perchlorate ion.
588 Chem. Eng. J. 191, 141–146. https://doi.org/10.1016/j.cej.2012.02.085

589 França, D.B., Torres, S.M., Filho, E.C.S., Fonseca, M.G., Jaber, M., 2019. Understanding the
590 interactions between ranitidine and magadiite: Influence of the interlayer cation.
591 Chemosphere 222, 980–990. https://doi.org/10.1016/j.chemosphere.2019.01.154

592 Freundlich, H.M.F., 1906. Over the adsorption in solution. J. Phys. Chem. 57, 385–471.

593 Ghemit, R., Makhloufi, A., Djebri, N., Flilissa, A., Zerroual, L., Boutahala, M., 2019.
594 Adsorptive removal of diclofenac and ibuprofen from aqueous solution by
595 organobentonites: Study in single and binary systems. Groundw. Sustain. Dev. 8, 520–
596 529. https://doi.org/10.1016/J.GSD.2019.02.004

597 Greenland, D.J., Quirk, J.P., 1962. Adsorption of 1-n-alkyl pyridinium bromides by
598 montmorillonite. Clays Clay Miner. 9, 484–499.

599 Gu, Z., Gao, M., Luo, Z., Lu, L., Ye, Y., Liu, Y., 2014. Bis-pyridinium dibromides modified
600 organo-bentonite for the removal of aniline from wastewater : A positive role of π-π
601 polar interaction. Appl. Surf. Sci. 290, 107–115.
602 https://doi.org/10.1016/j.apsusc.2013.11.008

603 He, B., Wang, J., Liu, J., Hu, X., 2017. Eco-pharmacovigilance of non-steroidal anti-
604 inflammatory drugs: Necessity and opportunities. Chemosphere 181, 178–189.
605 https://doi.org/10.1016/J.CHEMOSPHERE.2017.04.084

He, H., Ma, L., Zhu, J., Frost, R.L., Theng, B.K.G., Bergaya, F., 2014. Synthesis of organoclays: A critical review and some unresolved issues. Appl. Clay Sci. 100, 22–28. https://doi.org/10.1016/j.clay.2014.02.008

Herrera, P., Burghardt, R., Huebner, H.J., Phillips, T.D., 2004. The efficacy of sand-immobilized organoclays as filtration bed materials for bacteria. Food Microbiol. 21, 1–10. https://doi.org/10.1016/S0740-0020(03)00050-9

Herrera, P., Burghardt, R.C., Phillips, T.D., 2000. Adsorption of Salmonella enteritidis by cetylpyridinium-exchanged montmorillonite clays. Vet. Microbiol. 74, 259–272. https://doi.org/10.1016/S0378-1135(00)00157-7

Ho, Y.S., McKay, G., 1999. Pseudo-second order model for sorption processes. Process Biochem. 34, 451–465. https://doi.org/10.1016/S0032-9592(98)00112-5

Iliescu, T., Baia, M., Kiefer, W., 2004. FT-Raman, surface-enhanced Raman spectroscopy and theoretical investigations of diclofenac sodium. Chem. Phys. 298, 167–174. https://doi.org/10.1016/J.CHEMPHYS.2003.11.018

Jović-Jovičić, N., Mojović, M., Stanković, D., Nedić-Vasiljević, B., Milutinović-Nikolić, A., Banković, P., Mojović, Z., 2019. Characterization and electrochemical properties of organomodified and corresponding derived carbonized clay. Electrochim. Acta 296, 387–396. https://doi.org/10.1016/J.ELECTACTA.2018.11.031

Karaman, R., Khamis, M., Quried, M., Halabieh, R., Makharzeh, I., Manassra, A., Abbadi, J., Qtait, A., Bufod, S.A., Nasser, A., Nir, S., 2012. Removal of diclofenac potassium from wastewater using clay-micelle complex. Environ. Technol. 33, 1279–1287. https://doi.org/10.1080/09593330.2011.619582

Ke, Y.L., Jiao, L.F., Song, Z.H., Xiao, K., Lai, T.M., Lu, J.J., Hu, C.H., 2014. Effects of cetylpyridinium-montmorillonite, as alternative to antibiotic, on the growth performance, intestinal microflora and mucosal architecture of weaned pigs. Anim. Feed Sci. Technol. 198, 257–262. https://doi.org/10.1016/j.anifeedsci.2014.10.010

Klaudia, Ś., Szaniawska, A., Caban, M., 2019. Evaluation of bioconcentration and metabolism of diclofenac in mussels Mytilus trossulus - laboratory study. Mar. Pollut. Bull. J. 141, 249–255. https://doi.org/10.1016/j.marpolbul.2019.02.050

Kovala-Demertzi, D., Dimitris, M., Terzis, A., 1993. Metal complexes of the anti-inflammatory drug sodium [2-[(2, 6-dichlorophenyl) amino] phenyl] acetate (diclofenac sodium). Molecular and crystal structure of cadmium diclofenac. Polyhedron 12, 1361–1370. https://doi.org/org/10.1016/S0277-5387(00)84327-2

Lagaly, G., Ogawa, M., Dékány, I., 2013. Clay mineral–organic interactions, in: Bergaya, F., Lagaly, G. (Eds.), Handbook of Clay Science. Elsevier, Developments in Clay Science, Amsterdam, p. 435–505 (Chapter 10.3). https://doi.org/10.1016/B978-0-08-098258-8.00015-8

Lagergren, S., 1898. Zur theorie der sogenannten adsorption geloster kungliga svenska vetenskapsakdemiens. Handlingar 24, 1–39.

Langmuir, I., 1918. The adsorption of gases on plane surfaces of glass mica and platinum. J. Am. Chem. Soc. 40, 1361–1403. https://doi.org/10.1021/ja02242a004

Li, J., Zhu, L., Cai, W., 2006. Characteristics of organobentonite prepared by microwave as a sorbent to organic contaminants in water. Colloids Surfaces A Physicochem. Eng. Asp. 281, 177–183. https://doi.org/10.1016/j.colsurfa.2006.02.055

Lima, É.C., Adebayo, M.A., Machado, F.M., 2015. Kinetic and Equilibrium Models of Adsorption, in: Bergmann, C.P., Machado, F.M. (Eds.), Carbon Nanomaterials as Adsorbents for Environmental and Biological Applications. Springer, Cham, pp. 33–69. https://doi.org/10.1007/978-3-319-18875-1_3

Lin-Vien, D., Colthup, N.B., Fateley, W.G., Grasselli, J.G., 1991. The Handbook of infrared and raman characteristic frequencies of organic molecules, first. ed. Academic Press.

Lonappan, L., Kaur, S., Kumar, R., Verma, M., Surampalli, R.Y., 2016. Diclofenac and its transformation products : Environmental occurrence and toxicity - A review. Environ. Int. 96, 127–138. https://doi.org/10.1016/j.envint.2016.09.014

Luo, W., Hirajima, T., Sasaki, K., 2016. Optimization of hexadecylpyridinium-modified montmorillonite for removal of perchlorate based on adsorption mechanisms. Appl. Clay Sci. 123, 29–36. https://doi.org/10.1016/j.clay.2016.01.005

Luo, W., Inoue, A., Hirajima, T., Sasaki, K., 2017. Synergistic effect of Sr^{2+} and ReO_4^- adsorption on hexadecyl pyridinium-modified montmorillonite. Appl. Surf. Sci. 394, 431–439. https://doi.org/10.1016/j.apsusc.2016.10.135

Luo, W., Sasaki, K., Hirajima, T., 2018. Influence of the pre-dispersion of montmorillonite on organic modification and the adsorption of perchlorate and methyl red anions. Appl. Clay Sci. 154, 1–9. https://doi.org/10.1016/j.clay.2017.12.032

Luo, Z., Gao, M., Yang, S., Yang, Q., 2015. Adsorption of phenols on reduced-charge montmorillonites modified by bispyridinium dibromides: Mechanism , kinetics and thermodynamics studies. Colloids Surfaces A Physicochem. Eng. Asp. 482, 222–230. https://doi.org/10.1016/j.colsurfa.2015.05.014

Maia, G.S., Andrade, J.R., Silva, M.G.C., Vieira, M.G.A., 2019. Adsorption of diclofenac sodium onto commercial organoclay: Kinetic, equilibrium and thermodynamic study. Powder Technol. 345, 140–150. https://doi.org/10.1016/j.powtec.2018.12.097

Malachová, K., Praus, P., Pavlíčková, Z., Turicová, M., 2009. Activity of antibacterial compounds immobilised on montmorillonite. Appl. Clay Sci. 43, 364–368. https://doi.org/10.1016/J.CLAY.2008.11.003

Martinez-Costa, J.I., Leyva-Ramos, R., Padilla-Ortega, E., 2018. Sorption of diclofenac from aqueous solution on an organobentonite and adsorption of cadmium on organobentonite saturated with diclofenac. Clays Clay Miner. 66, 515–528. https://doi.org/10.1346/ccmn.2018.064119

Meleshyn, A., Bunnenberg, C., 2006. Interlayer expansion and mechanisms of anion sorption of Na-montmorillonite modified by cetylpyridinium chloride: A Monte Carlo study. J. Phys. Chem. B 110, 2271–2277. https://doi.org/10.1021/jp056178v

Momina, Shahadat, M., Isamil, S., 2018. Regeneration performance of clay-based adsorbents for the removal of industrial dyes: A review. RSC Adv. 8, 24571–24587. https://doi.org/10.1039/c8ra04290j

688 Moreno-González, R., Rodríguez-Mozaz, S., Huerta, B., Barceló, D., León, V.M., 2016. Do
689 pharmaceuticals bioaccumulate in marine molluscs and fish from a coastal lagoon?
690 Environ. Res. 146, 282–298. https://doi.org/10.1016/J.ENVRES.2016.01.001

691 Mugunthan, E., Saidutta, M.B., Jagadeeshbabu, P.E., 2018. Visible light assisted
692 photocatalytic degradation of diclofenac using TiO_2-WO_3 mixed oxide catalysts.
693 Environ. Nanotechnology, Monit. Manag. 10, 322–330.
694 https://doi.org/10.1016/J.ENMM.2018.07.012

695 Muñoz-Shugulí, C., Rodríguez, F.J., Bruna, J.E., Galotto, M.J., Sarantópoulos, C., Favaro
696 Perez, M.A., Padula, M., 2019. Cetylpyridinium bromide-modified montmorillonite as
697 filler in low density polyethylene nanocomposite films. Appl. Clay Sci. 168, 203–210.
698 https://doi.org/10.1016/j.clay.2018.10.020

699 Oaks, J.L., Gilbert, M., Virani, M.Z., Watson, R.T., Meteyer, C.U., Rideout, B.A.,
700 Shivaprasad, H.L., Ahmed, S., Iqbal Chaudhry, M.J., Arshad, M., Mahmood, S., Ali, A.,
701 Ahmed Khan, A., 2004. Diclofenac residues as the cause of vulture population decline in
702 Pakistan. Nature 427, 630–633. https://doi.org/10.1038/nature02317

703 Oliveira, T. De, Guégan, R., Thiebault, T., Le, C., Muller, F., Teixeira, V., Giovanela, M.,
704 Boussafir, M., 2017. Adsorption of diclofenac onto organoclays: Effects of surfactant
705 and environmental (pH and temperature) conditions. J. Hazard. Mater. 323, 558–566.
706 https://doi.org/10.1016/j.jhazmat.2016.05.001

707 Oliveira, T., Guégan, R., 2016. Coupled organoclay/micelle action for the adsorption of
708 diclofenac. Environ. Sci. Technol. 50, 10209–10215.
709 https://doi.org/10.1021/acs.est.6b03393

710 Özdemir, G., Yapar, S., Limoncu, M.H., 2013. Preparation of cetylpyridinium
711 montmorillonite for antibacterial applications. Appl. Clay Sci. 72, 201–205.
712 https://doi.org/10.1016/j.clay.2013.01.010

713 Pérez-Estrada, L.A., Malato, S., Gernjak, W., Agüera, A., Thurman, E.M., Ferrer, I.,
714 Fernández-Alba, A.R., 2005. Photo-fenton degradation of diclofenac: Identification of
715 main intermediates and degradation pathway. Environ. Sci. Technol. 39, 8300–8306.
716 https://doi.org/10.1021/ES050794N

717 Queiroga, L.N.F., Pereira, M.B.B., Silva, L.S., Silva Filho, E.C., Santos, I.M.G., Fonseca,
718 M.G., Georgelin, T., Jaber, M., 2019. Microwave bentonite silylation for dye removal:
719 Influence of the solvent. Appl. Clay Sci. 168, 478–487.
720 https://doi.org/10.1016/j.clay.2018.11.027

721 Sarkar, B., Megharaj, M., Shanmuganathan, D., Naidu, R., 2013. Toxicity of organoclays to
722 microbial processes and earthworm survival in soils. J. Hazard. Mater. 261, 793–800.
723 https://doi.org/10.1016/J.JHAZMAT.2012.11.061

724 Schampera, B., Dultz, S., 2009. Determination of diffusive transport in HDPy-
725 montmorillonite by H_2O-D_2O exchange using in situ ATR-FTIR spectroscopy. Clay
726 Miner. 44, 249–266. https://doi.org/10.1180/claymin.2009.044.2.249

727 Scheurell, M., Franke, S., Shah, R.M., Hühnerfuss, H., 2009. Occurrence of diclofenac and its
728 metabolites in surface water and effluent samples from Karachi, Pakistan. Chemosphere
729 77, 870–876. https://doi.org/10.1016/J.CHEMOSPHERE.2009.07.066

730 Skoog, D.A., West, D.M., Holler, F.J., Crouch, S.R., 2012. Fundamentals of analytical
731 chemistry.

732 Slaný, M., Jankovič, Ľ., Madejová, J., 2019. Structural characterization of organo-
733 montmorillonites prepared from a series of primary alkylamines salts: Mid-IR and near-
734 IR study. Appl. Clay Sci. 176, 11–20. https://doi.org/10.1016/j.clay.2019.04.016

735 Starling, M.C.V.M., Amorim, C.C., Leão, M.M.D., 2019. Occurrence, control and fate of
736 contaminants of emerging concern in environmental compartments in Brazil. J. Hazard.
737 Mater. 372, 17–36. https://doi.org/10.1016/J.JHAZMAT.2018.04.043

738 Sun, K., Shi, Y., Chen, H., Wang, X., Li, Z., 2017a. Extending surfactant-modified 2:1 clay
739 minerals for the uptake and removal of diclofenac from water. J. Hazard. Mater. 323,
740 567–574. https://doi.org/10.1016/j.jhazmat.2016.05.038

741 Sun, K., Shi, Y., Wang, X., Li, Z., 2017b. Sorption and retention of diclofenac on zeolite in
742 the presence of cationic surfactant. J. Hazard. Mater. 323, 584–592.
743 https://doi.org/10.1016/j.jhazmat.2016.08.026

744 Sun, K., Shi, Y., Wang, X., Rasmussen, J., Li, Z., Zhu, J., 2017c. Organokaolin for the uptake
745 of pharmaceuticals diclofenac and chloramphenicol from water. Chem. Eng. J. 330,
746 1128–1136. https://doi.org/10.1016/j.cej.2017.08.057

747 Temkin, M.J., Pyzhev, V., 1940. Recent modifications to Langmuir isotherms. Acta
748 Physicochim. USSR 12, 217–222.

749 Teppen, B.J., Aggarwal, V., 2007. Thermodynamics of organic cation exchange selectivity in
750 smectites. Clays Clay Miner. 55, 119–130. https://doi.org/10.1346/CCMN.2007.0550201

751 Thanhmingliana, D.T., 2015. Efficient use of hybrid materials in the remediation of aquatic
752 environment contaminated with micro-pollutant diclofenac sodium. Chem. Eng. J. 263,
753 364–373. https://doi.org/10.1016/j.cej.2014.10.102

754 Vieno, N., Sillanpää, M., 2014. Fate of diclofenac in municipal wastewater treatment plant —
755 A review. Environ. Int. 69, 28–39. https://doi.org/10.1016/J.ENVINT.2014.03.021

756 Volzone, C., Rinaldi, J.O., Ortiga, J., 2002. N_2 and CO_2 Adsorption by TMA-and HDP-
757 Montmorillonites. Mater. Res. 5, 475–479. https://doi.org/10.1590/S1516-
758 14392002000400013

759 Witthuhn, B., Klauth, P., Klumpp, E., Narres, H.D., Martinius, H., 2005. Sorption and
760 biodegradation of 2,4-dichlorophenol in the presence of organoclays. Appl. Clay Sci. 28,
761 55–66. https://doi.org/10.1016/j.clay.2004.01.003

762 Yang, Q., Gao, M., Luo, Z., Yang, S., 2016. Enhanced removal of bisphenol A from aqueous
763 solution by organo-montmorillonites modified with novel Gemini pyridinium surfactants
764 containing long alkyl chain. Chem. Eng. J. 285, 27–38.
765 https://doi.org/10.1016/j.cej.2015.09.114

766 Yapar, S., 2009. Physicochemical study of microwave-synthesized organoclays. Colloids
767 Surfaces A Physicochem. Eng. Asp. 345, 75–81.
768 https://doi.org/10.1016/j.colsurfa.2009.04.032

769 Zhu, L., Tian, S., Shi, Y., 2005. Adsorption of volatile organic compounds onto porous clay

heterostructures based on spent organobentonites. Clays Clay Miner. 53, 123–136. https://doi.org/10.1346/CCMN.2005.0530202

Zhuang, G., Zhang, Z., Jaber, M., 2019. Organoclays used as colloidal and rheological additives in oil-based drilling fluids: An overview. Appl. Clay Sci. 177, 63–81. https://doi.org/10.1016/J.CLAY.2019.05.006

Zhuang, G., Zhang, Z., Peng, S., Gao, J., Jaber, M., 2018. Enhancing the rheological properties and thermal stability of oil-based drilling fluids by synergetic use of organo-montmorillonite and organo-sepiolite. Appl. Clay Sci. 161, 505–512. https://doi.org/10.1016/J.CLAY.2018.05.018

Figure captions

Figure 1 - Equilibrium isotherms and their fitting to the Langmuir, Freundlich and Temkin models for sodium diclofenac adsorption on a) Bent-C_{12}py-100%, (b) Bent-C_{16}py-100%, (c) Bent-C_{12}py-200% and (d) Bent-C_{16}py-200% at 25 °C and pH 6.0.

795 Figure 2 – XRD patterns of organobentonites for (i) Bent-C_{12}py-100%, (ii) Bent-C_{16}py-100%,
796 (iii) Bent-C_{12}py-200% and (iv) Bent-C_{16}py-200% (a) before and after diclofenac adsorption
797 for hybrids prepared with initial drug concentrations of (b) 10 mg L^{-1}, (c) 100 mg L^{-1} and (d)
798 500 mg L^{-1}.

799

800 Figure 3 – FTIR results for a) Bent-C_{16}py-200% before and after diclofenac sorption using
801 initial concentrations of b) 10 mg L^{-1}, c) 100 mg L^{-1} and d) 500 mg L^{-1}; and e) free diclofenac
802 sodium.

803

804 Figure 4 - Proposed scheme for diclofenac/organobentonite interaction, M = mechanism.

805

806

807

808

809

810

811

812

813

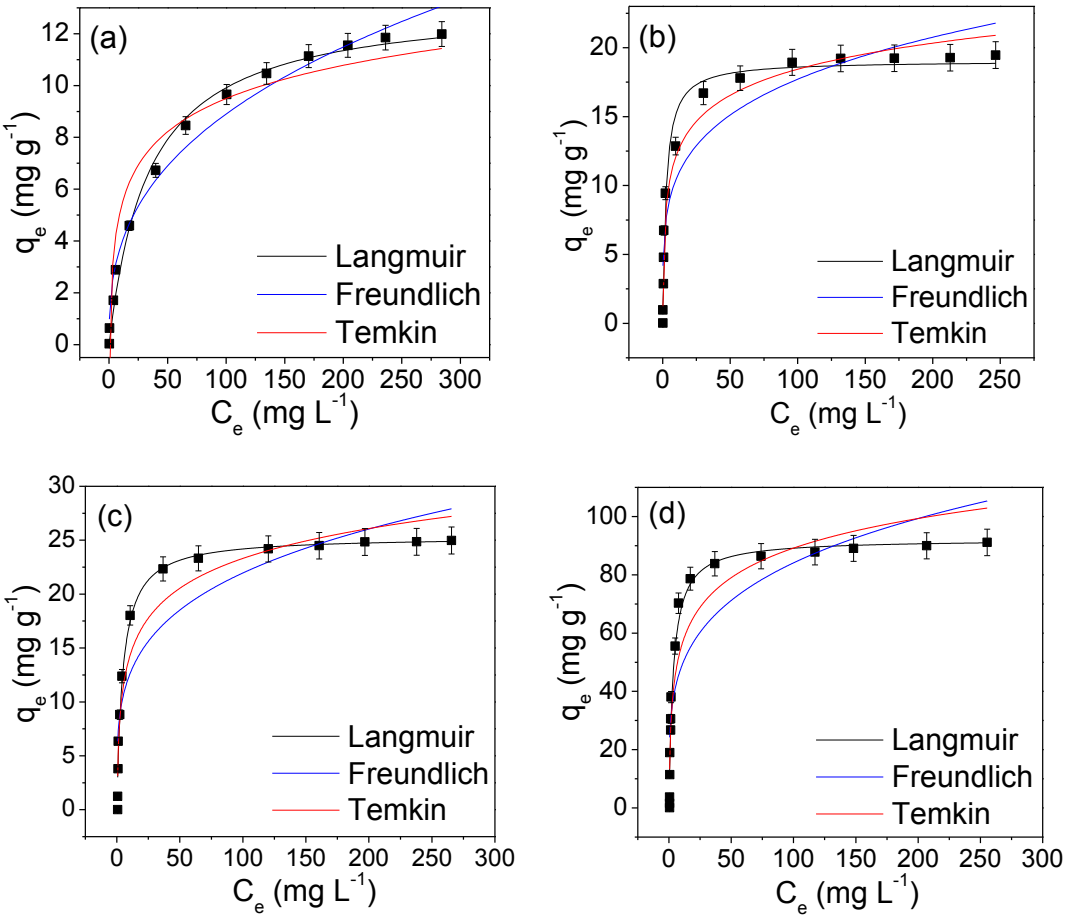

Figure 1

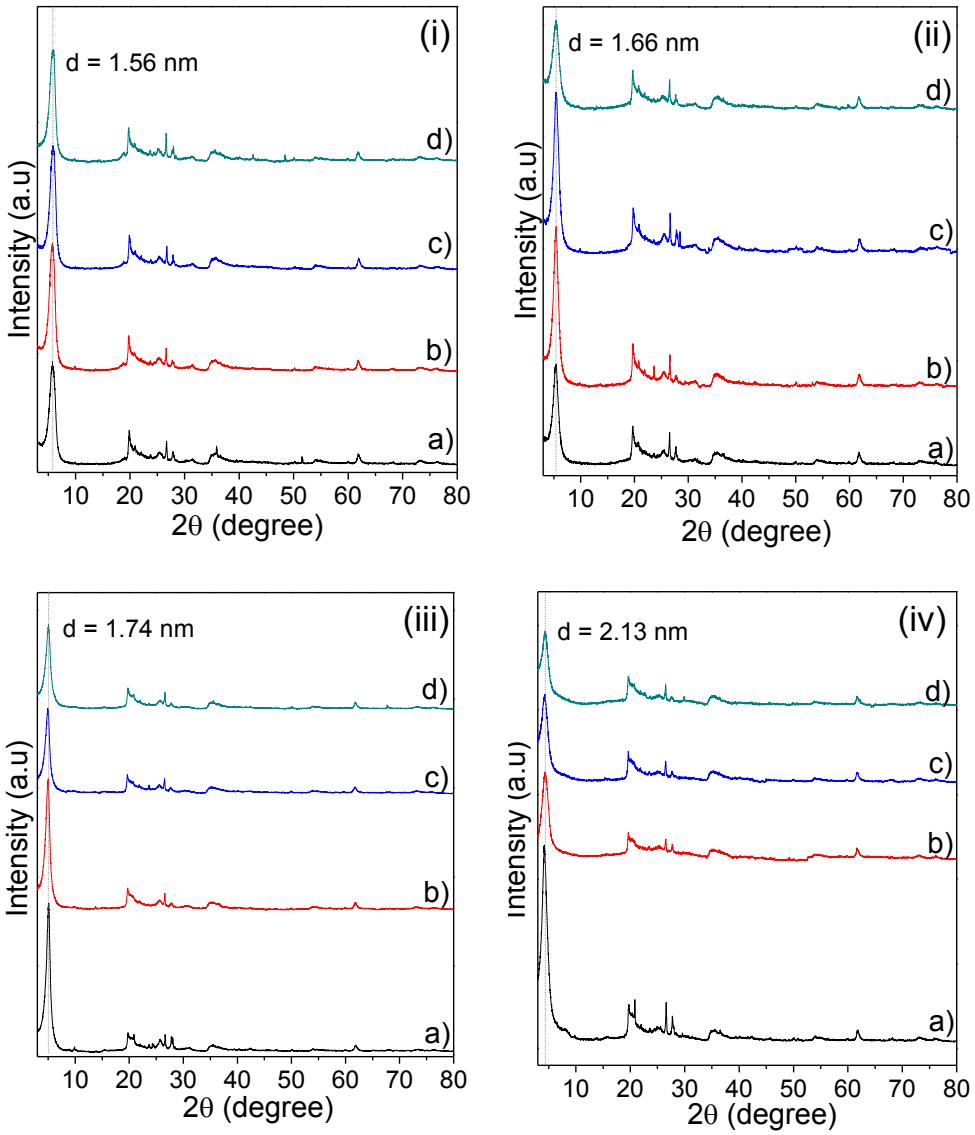
(i)
d = 1.56 nm
d)
c)
b)
a)
Intensity (a.u)
10 20 30 40 50 60 70 80
2θ (degree)
(ii)
d = 1.66 nm
d)
c)
b)
a)
Intensity (a.u)
10 20 30 40 50 60 70 80
2θ (degree)
(iii)
d = 1.74 nm
d)
c)
b)
a)
Intensity (a.u)
10 20 30 40 50 60 70 80
2θ (degree)
(iv)
d = 2.13 nm
d)
c)
b)
a)
Intensity (a.u)
10 20 30 40 50 60 70 80
2θ (degree)

Figure 2

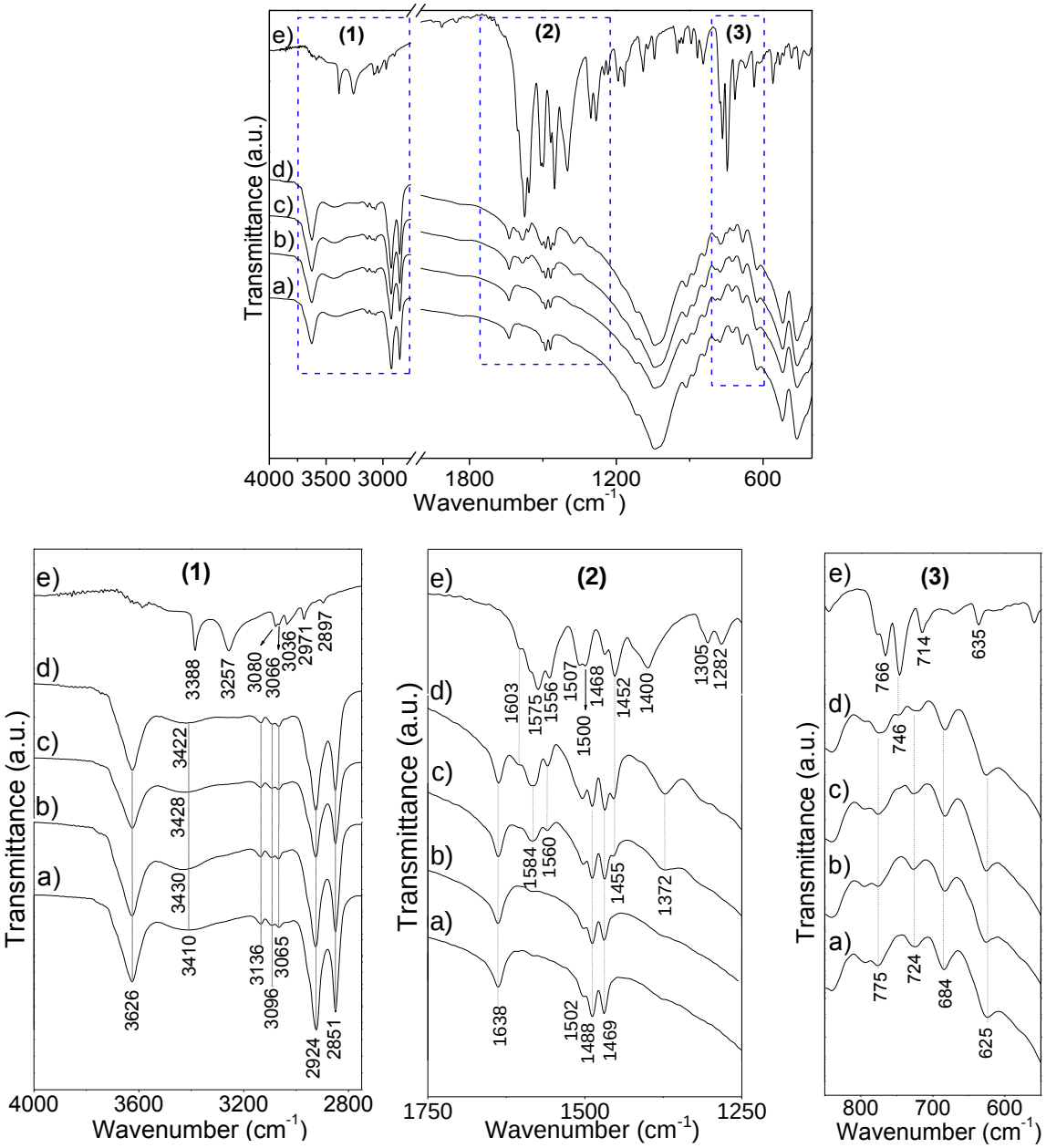

831

832 **Figure 3**

833

834

835

836

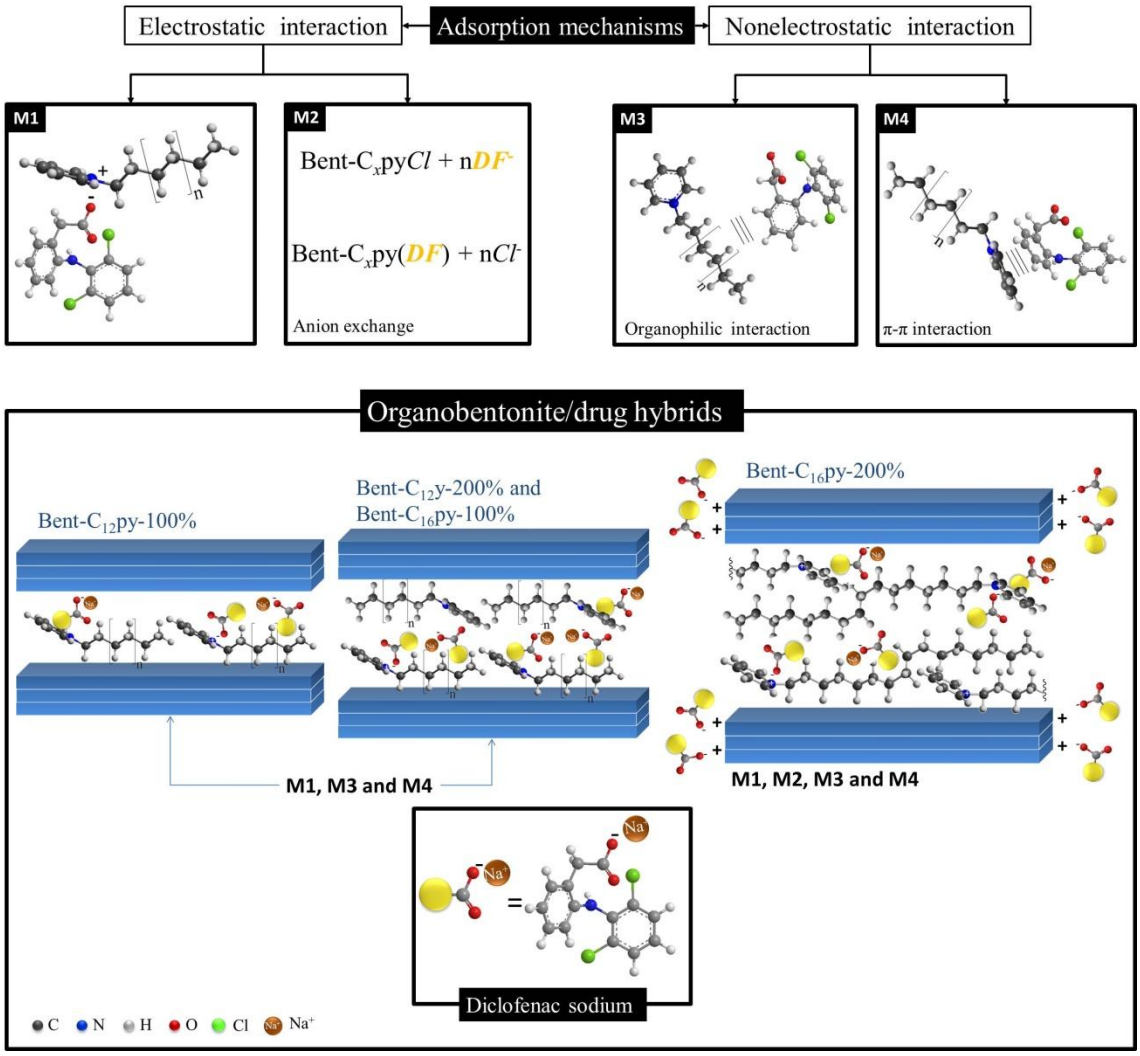
Electrostatic interaction
Adsorption mechanisms
Nonelectrostatic interaction
M1
M2
Bent-C$_x$pyCl + nDF$^-$
Bent-C$_x$py(DF) + nCl$^-$
Anion exchange
M3
Organophilic interaction
M4
π-π interaction
Organobentonite/drug hybrids
Bent-C$_{12}$py-100%
Bent-C$_{12}$y-200% and
Bent-C$_{16}$py-100%
Bent-C$_{16}$py-200%
M1, M3 and M4
M1, M2, M3 and M4
Diclofenac sodium
C N H O Cl Na$^+$

Figure 4

Graphical abstract

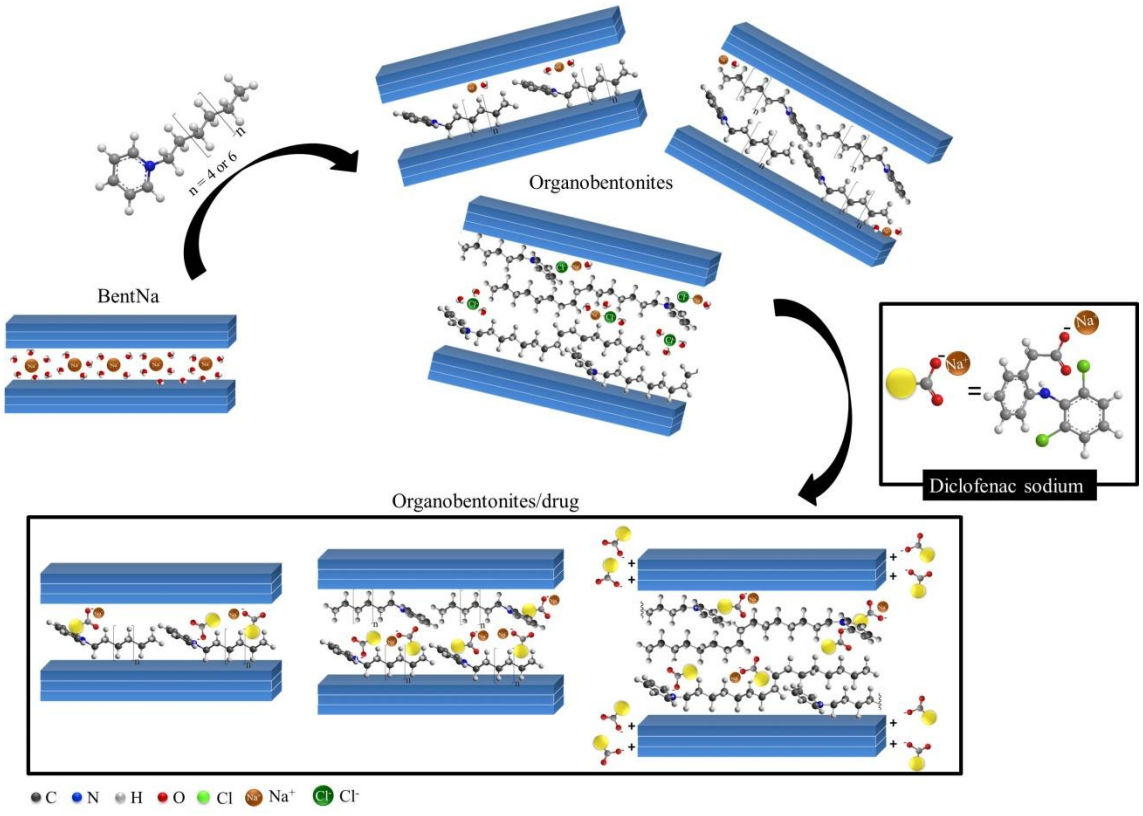

Table 1 – C, N and Cl elemental analysis of organobentonites and percentage of incorporated surfactant in relation to the CEC of BentNa (σ_f).

Sample	C		N		σ_f	Cl^-
	%	mmol g^{-1}	%	mmol g^{-1}	%	mmol g^{-1}
Bent-C_{12}py-100%	12.30	10.25	0.93	0.66	89.0	*
Bent-C_{16}py-100%	15.75	13.13	0.97	0.69	92.8	*
Bent-C_{12}py-200%	14.85	12.38	0.98	0.70	93.3	*
Bent-C_{16}py-200%	20.85	17.37	1.18	0.84	112.4	0.15 ± 0.01

*null for all

Table 2 – Kinetic parameters obtained from the pseudo-first-order, pseudo-second-order and Elovich equations in nonlinear fitting of diclofenac adsorption on organophilic bentonites (Experimental conditions: 25 °C, pH 6.0 and 100 mg L^{-1} diclofenac solution).

Pseudo-first-order					
Solid	$q_{e(exp)}$ (mg g^{-1})	k_1 (min^{-1})	$q_{e(cal)}$ (mg g^{-1})	R^2	SD (mg g^{-1})
Bent-C_{12}py-100%	5.50 ± 0.10	2.84 ± 0.65	5.01 ± 0.13	0.9242	0.410
Bent-C_{16}py-100%	8.98 ± 0.27	3.54 ± 0.82	8.36 ± 0.20	0.9573	0.554
Bent-C_{12}py-200%	12.98 ± 0.05	2.18 ± 0.12	12.80 ± 0.09	0.9938	0.293
Bent-C_{16}py-200%	38.71 ± 0.04	4.06 ± 0.33	38.53 ± 0.27	0.9950	0.814
Pseudo-second-order					
Solid	$q_{e(exp)}$ (mg g^{-1})	k_2 (g mg^{-1} min^{-1})	$q_{e(cal)}$ (mg g^{-1})	R^2	SD (mg g^{-1})
Bent-C_{12}py-100%	5.50 ± 0.10	0.99 ± 0.25	5.18 ± 0.11	0.9641	0.282
Bent-C_{16}py-100%	8.98 ± 0.27	0.81 ± 0.25	8.54 ± 0.16	0.9752	0.422
Bent-C_{12}py-200%	12.98 ± 0.05	0.35 ± 0.01	13.06 ± 0.05	0.9985	0.141
Bent-C_{16}py-200%	38.71 ± 0.04	0.33 ± 0.02	38.95 ± 0.11	0.9993	0.308
Elovich					
Solid	α (10^6 mg g^{-1} min^{-1})		β (g mg^{-1})	R^2	SD (mg g^{-1})
Bent-C_{12}py-100%	1.07 ± 0.66		3.56 ± 0.13	0.9983	0.061
Bent-C_{16}py-100%	44.5 ± 33.4		2.57 ± 0.09	0.9992	0.076
Bent-C_{12}py-200%	84.97 ± 377.04		1.73 ± 0.38	0.9622	0.727
Bent-C_{16}py-200%	9.48 10^{15} ± 133.78 10^{15}		1.40 ± 0.37	0.9915	1.061

887 Table 3 – Adsorption parameters of diclofenac on organophilic bentonites at 25 °C and pH 6.0
888 according to the Langmuir, Freundlich and Temkin models.
889

Langmuir					
Solid	$q_{e\ (exp)}$ (mg g^{-1})	q_{max} (mg g^{-1})	K_L (10^{-1} L mg^{-1})	R^2	SD (mg g^{-1})
Bent-C_{12}py-100%	13.02 ± 0.65	13.26 ± 0.35	0.30 ± 0.03	0.9917	0.41
Bent-C_{16}py-100%	19.30 ± 0.96	19.05 ± 0.43	4.00 ± 0.56	0.9806	1.05
Bent-C_{12}py-200%	25.50 ± 1.02	25.33 ± 0.53	2.11 ± 0.24	0.9843	1.23
Bent-C_{16}py-200%	91.13 ± 1.82	92.20 ± 2.68	2.91 ± 0.39	0.9704	6.15
Freundlich					
Solid	n	K_f (mg g^{-1})(mg L^{-1})$^{-1/n}$	R^2		SD (mg g^{-1})
Bent-C_{12}py-100%	2.71 ± 0.21	1.63 ± 0.23	0.9767		0.70
Bent-C_{16}py-100%	4.37 ± 0.60	6.17 ± 0.91	0.8943		2.47
Bent-C_{12}py-200%	4.10 ± 0.65	7.10 ± 1.33	0.8533		3.76
Bent-C_{16}py-200%	4.16 ± 0.67	27.82 ± 4.81	0.7961		16.14
Temkin					
Solid	b_T (10^2 J mol^{-1})	A_T (L mg^{-1})	R^2		SD (mg g^{-1})
Bent-C_{12}py-100%	13.61 ± 1.02	1.70 ± 0.56	0.9366		1.31
Bent-C_{16}py-100%	9.22 ± 0.40	8.60 ± 1.90	0.9766		1.16
Bent-C_{12}py-200%	6.20 ± 0.40	3.43 ± 0.99	0.9498		2.20
Bent-C_{16}py-200%	1.70 ± 0.13	4.41 ± 1.38	0.9156		10.38

890